




# Comparative Investigation into Formycin A and Pyrazofurin A Biosynthesis Reveals Branch Pathways for the Construction of C-Nucleoside Scaffolds

Meng Zhang,<sup>a</sup> Peichao Zhang,<sup>a,b</sup> Gudan Xu,<sup>a</sup> Wenting Zhou,<sup>a</sup> Yaojie Gao,<sup>a</sup> Rong Gong,<sup>a</sup> You-Sheng Cai,<sup>a</sup> Hengjiang Cong,<sup>c</sup> Zixin Deng,<sup>a</sup> Neil P. J. Price,<sup>d</sup> Xiangzhao Mao,<sup>b</sup>  Wenqing Chen<sup>a</sup>

<sup>a</sup>Key Laboratory of Combinatorial Biosynthesis and Drug Discovery, Ministry of Education, and School of Pharmaceutical Sciences, Wuhan University, Wuhan, China

<sup>b</sup>College of Food Science and Engineering, Ocean University of China, Qingdao, China

<sup>c</sup>College of Chemistry and Molecular Sciences, Institute for Advanced Studies, Wuhan University, Wuhan, China

<sup>d</sup>Agricultural Research Service, U.S. Department of Agriculture, National Center for Agricultural Utilization Research, Peoria, Illinois, USA

Meng Zhang, Peichao Zhang, and Gudan Xu contributed equally to this paper.

**ABSTRACT** Formycin A (FOR-A) and pyrazofurin A (PRF-A) are purine-related C-nucleoside antibiotics in which ribose and a pyrazole-derived base are linked by a C-glycosidic bond. However, the logic underlying the biosynthesis of these molecules has remained largely unexplored. Here, we report the discovery of the pathways for FOR-A and PRF-A biosynthesis from diverse actinobacteria and propose that their biosynthesis is likely initiated by a lysine *N*<sup>6</sup>-monooxygenase. Moreover, we show that *forT* and *prfT* (involved in FOR-A and PRF-A biosynthesis, respectively) mutants are correspondingly capable of accumulating the unexpected pyrazole-related intermediates 4-amino-3,5-dicarboxypyrazole and 3,5-dicarboxy-4-oxo-4,5-dihydropyrazole. We also decipher the enzymatic mechanism of ForT/PrfT for C-glycosidic bond formation in FOR-A/PRF-A biosynthesis. To our knowledge, ForT/PrfT represents an example of  $\beta$ -RFA-P ( $\beta$ -ribofuranosyl-aminobenzene 5'-phosphate) synthase-like enzymes governing C-nucleoside scaffold construction in natural product biosynthesis. These data establish a foundation for combinatorial biosynthesis of related purine nucleoside antibiotics and also open the way for target-directed genome mining of PRF-A/FOR-A-related antibiotics.

**IMPORTANCE** FOR-A and PRF-A are C-nucleoside antibiotics known for their unusual chemical structures and remarkable biological activities. Deciphering the enzymatic mechanism for the construction of a C-nucleoside scaffold during FOR-A/PRF-A biosynthesis will not only expand the biochemical repertoire for novel enzymatic reactions but also permit target-oriented genome mining of FOR-A/PRF-A-related C-nucleoside antibiotics. Moreover, the availability of FOR-A/PRF-A biosynthetic gene clusters will pave the way for the rational generation of designer FOR-A/PRF-A derivatives with enhanced/selective bioactivity via synthetic biology strategies.

**KEYWORDS** C-nucleoside antibiotics, monooxygenase, C-glycosidic bond, combinatorial biosynthesis, genome mining

The naturally occurring C-nucleosides formycin A (FOR-A) and pyrazofurin A (PRF-A) (Fig. 1) are unusual biological molecules in which the base and ribosyl moieties are linked via a structurally conserved C-glycosidic bond (1, 2). Other important C-nucleoside antibiotics in this group include showdomycin (3) and pseudouridimycin (4) (Fig. 1). The pathway for showdomycin biosynthesis was discovered by relying on the use of the genes encoding the enzyme pair AlnA (C-glycosyltransferase) and AlnB (phosphatase) as a probe. These two enzymes catalyze the formation of the C-ribosylated aromatic polyketide alnumycin C in a

**Citation** Zhang M, Zhang P, Xu G, Zhou W, Gao Y, Gong R, Cai Y-S, Cong H, Deng Z, Price NPJ, Mao X, Chen W. 2020. Comparative investigation into formycin A and pyrazofurin A biosynthesis reveals branch pathways for the construction of C-nucleoside scaffolds. *Appl Environ Microbiol* 86:e01971-19. <https://doi.org/10.1128/AEM.01971-19>.

**Editor** Claire Vieille, Michigan State University

**Copyright** © 2020 American Society for Microbiology. All Rights Reserved.

Address correspondence to Wenqing Chen, [wqchen@whu.edu.cn](mailto:wqchen@whu.edu.cn), or Xiangzhao Mao, [xzhmao@ouc.edu.cn](mailto:xzhmao@ouc.edu.cn).

**Received** 27 August 2019

**Accepted** 25 October 2019

**Accepted manuscript posted online** 1 November 2019

**Published** 7 January 2020

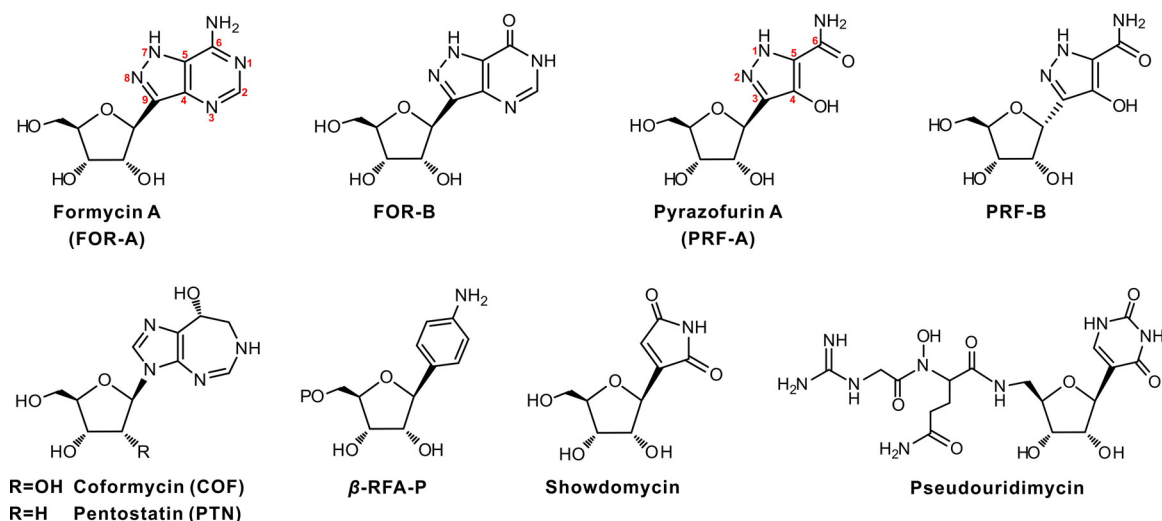


**FIG 1** Chemical structures of FOR-A, PRF-A, and related compounds.  $\beta$ -RFA-P,  $\beta$ -ribofuranosyl-aminobenzene 5'-phosphate.

two-step process (3). Recently, Sosio et al. identified the pseudouridimycin biosynthetic gene cluster by searching for the gene (contained in a gene cluster) encoding pseudouridine synthase (4).

FOR-A was originally isolated from the broth of *Nocardia interforma* in the process of screening for antitumor compounds (5), and later, this antibiotic, accompanied by FOR-B (a deaminated product of FOR-A) (Fig. 1), was discovered to be produced by *Streptomyces lavendulae* (6). FOR-A and FOR-B (particularly the latter) show bioactivities against *Xanthomonas oryzae*, a bacterial pathogen that causes rice plant disease, and influenza A virus, while only FOR-A shows antitumor and antiviral activities (7). Subsequently, FOR-A and coformycin (COF) (an adenosine deaminase inhibitor harboring a 1,3-diazepine ring) (Fig. 1) were found to be concomitantly produced by *Nocardia interforma* ATCC 21072 and *Streptomyces kaniharaensis* SF-557 (ATCC 21070) (8). This intriguing cobiosynthetic phenomenon has also been documented for other purine nucleoside antibiotic pairs, including pentostatin (PTN) and arabinofuranosyl adenine (produced by *Streptomyces antibioticus* NRRL 3238) (9), 2'-chloropentostatin and 2'-amino-2'-deoxyadenosine (produced by *Actinomadura* sp. strain ATCC 39365) (10), and fungus-produced PTN and cordycepin (11). These antibiotic pairs all employ an unusual but general protector-protégé strategy; i.e., PTN may protect arabinofuranosyl adenine (taking this antibiotic pair as an example) from deamination by the housekeeping adenosine deaminase (9–11).

PRF-A, produced by *Streptomyces candidus* NRRL 3601, possesses prominent antiviral and antitumor activities, but interestingly, PRF-B (Fig. 1), the  $\alpha$ -anomer of PRF-A coproduced by this strain in a smaller amount, shows little bioactivity (12). Previous studies indicated that PRF-A blocks the *de novo* biosynthesis of pyrimidine and purine by independently targeting orotidylate decarboxylase (13) and 5-aminoimidazole-4-carboxamide ribonucleotide formyltransferase (14).

Previous isotope feeding experiments demonstrated that glutamate and ribose play key roles in the C-glycosidic bond formation of FOR-A and indicated that the C-3-to-C-6 unit of PRF-A (C-9, C-4, C-5, and C-6 of FOR-A) is derived from C-4 to C-1 of glutamate and/or  $\alpha$ -ketoglutarate (15). Moreover, Ochi et al. confirmed that N-3, N-7, and N-8 of FOR-A originate from the  $\epsilon$ -amino nitrogen of lysine (16). More recently, Wang et al. identified the FOR-A biosynthetic gene cluster on the basis of previous studies (17) and deciphered the late steps to FOR-A biosynthesis, by which they established that FOR-A biosynthesis shares cross talk with the *de novo* purine pathway (17). Although a pathway for FOR-A biosynthesis was tentatively proposed, several important aspects still remained unknown.

In the present work, we report the identification and comparative analysis of the FOR-A/PRF-A biosynthetic gene clusters from diverse actinobacteria and further propose that the biosynthesis of FOR-A/PRF-A is likely initiated by a lysine  $N^6$ -monooxygenase. We also demonstrate that a  $\beta$ -RFA-P ( $\beta$ -ribofuranosyl-aminobenzene 5'-phosphate) synthase-like enzyme governs the construction of the C-glycosidic bond of FOR-A/PRF-A associated with cryptic decarboxylation.

## RESULTS

**Identification of FOR-A gene clusters from diverse actinobacteria.** COF and PTN, which have a significant structural resemblance, were recently revealed to share highly similar biosynthetic pathways (18). To identify the target gene clusters for FOR-A biosynthesis, we sequenced the genomes of *Nocardia interforma* ATCC 21072 and *S. kaniharaensis* ATCC 21070 using the Illumina method, which rendered ca. 9.3 Mb (*Nocardia interforma* ATCC 21072) and ca. 8.6 Mb (*S. kaniharaensis* ATCC 21070) of nonredundant bases after the assembly of clean reads. We then utilized PenB (short-chain dehydrogenase) and PenC (phosphoribosylaminoimidazole-succinocarboxamide synthetase), the key enzymes for PTN biosynthesis, as query sequences to perform a BLASTP analysis (9), and the target *foc* and *cof* gene clusters, encoding the enzymes denoted Foc2/CofA (66%/49% identity to PenB) and Foc1/CofB (69%/62% identity to PenC) (Fig. 2A; see also Table S1 in the supplemental material), respectively, were detected by genome mining of *Nocardia interforma* ATCC 21072 and *S. kaniharaensis* ATCC 21070. To correlate the *foc* gene cluster with FOR-A biosynthesis, we deleted a 1.8-kb region (containing *focI*, *foc1*, and *foc2*) (Fig. S1A and Table S1). After confirmation (Fig. S1B), the resultant mutant was fermented for metabolite analysis, and high-performance liquid chromatography (HPLC) and liquid chromatography–high-resolution mass spectrometry (LC-HRMS) analyses indicated that the production of FOR-A and COF was abolished in the PC1 mutant (Fig. 2B and C and Fig. S1C), confirming the identity of the *foc* gene cluster for the biosynthesis of the COF–FOR-A pair.

Further bioinformatic analysis led to the discovery of potential FOR-A gene clusters with organizational diversities from other actinobacterial strains, including *Streptomyces resistomycificus* NRRL 2290 and *Salinispora arenicola* CNS-205 (Fig. S1D). We then fermented these strains for metabolite analysis, and the HPLC and LC-mass spectrometry (MS) results indicated that *S. resistomycificus* NRRL 2290, but not *Salinispora arenicola* CNS-205, is capable of synthesizing FOR-A under the chosen fermentation conditions (Fig. S1E to G). These data suggested that FOR-A gene clusters highlighting organizational diversities are widely distributed among actinobacteria but that not all of these strains are conferred the ability for FOR-A production.

**Discovery of the PRF-A gene cluster from *S. candidus* NRRL 3601.** PRF-A is structurally similar to FOR-A, which implies that both molecules should employ similar enzymatic logics for the construction of the pyrazole ring. To search for the candidate gene cluster for PRF-A biosynthesis, we sequenced the genome of *S. candidus* NRRL 3601, generating ca. 8.3 Mb of nonredundant bases after the assembly of preliminary data, and we then used FocJ (methionine-tRNA ligase) as the query sequence to perform a BLASTP analysis, in that the function of Spb40 (FocJ homolog) from the s56-p1 (a dipeptide natural product) pathway was recently confirmed for *N-N* bond formation (19). This approach leads to the location of a candidate gene cluster from the *S. candidus* NRRL 3601 genome, encoding PrfJ (86%/58% identities to FocJ/ForJ), PrfK (L-lysine  $N^6$ -monooxygenase) (84%/62% identities to FocK/ForK), and Prf1 (phosphoribosylaminoimidazole-succinocarboxamide synthetase) (82%/60% identities to Foc1/CofB) (Fig. 2A, Table 1, and Table S1). This strongly suggested that the target gene cluster is involved in PRF-A biosynthesis.

**Comparative analysis of the gene clusters for FOR-A and PRF-A biosynthesis.** Comparative analysis of the FOR-A gene clusters revealed that they have apparent diversities in genetic organization as well as in the total number of genes. The FOR-A gene cluster (30 genes) from *S. kaniharaensis* ATCC 21070 spans a 37.0-kb continuous

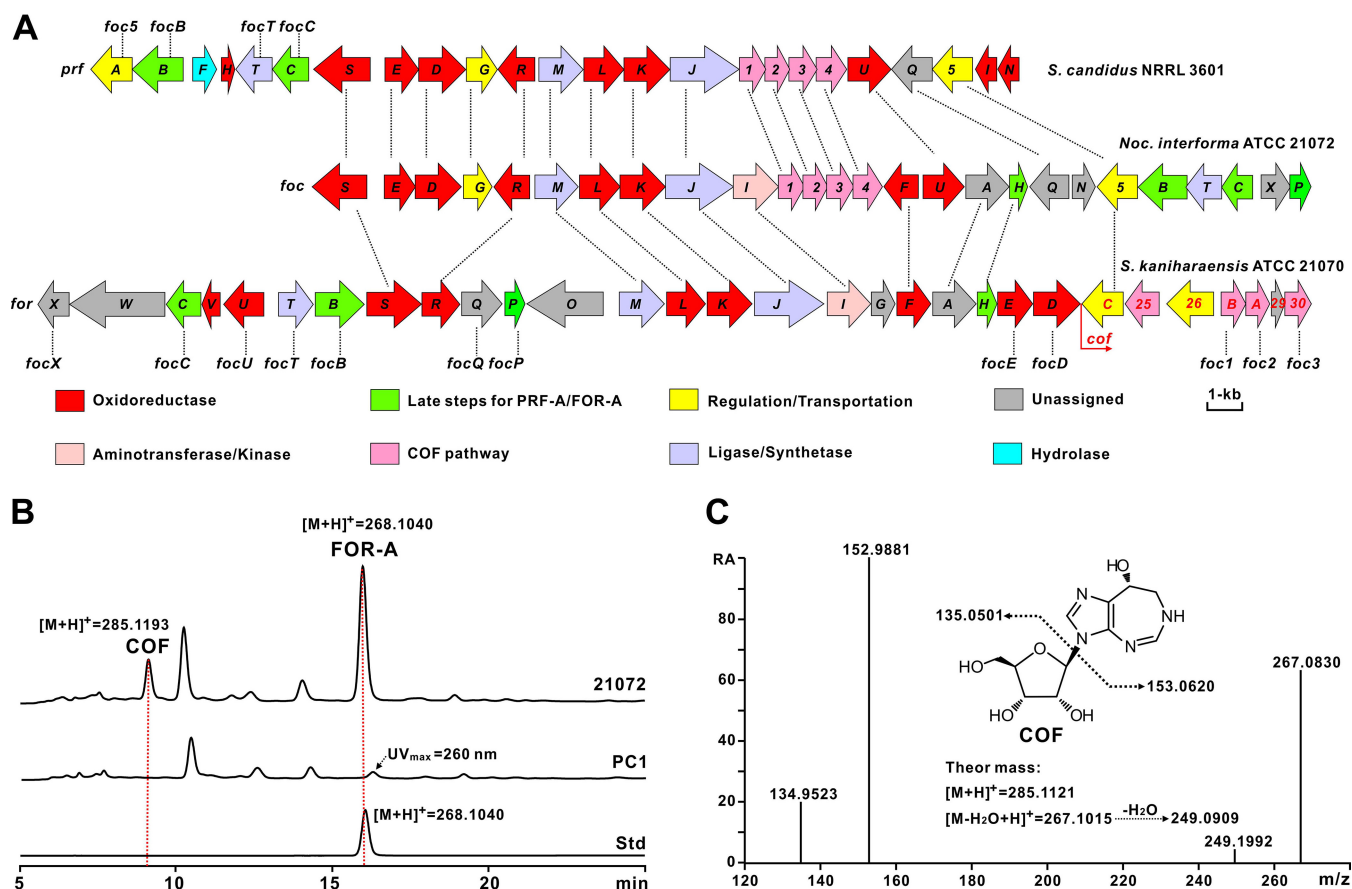


**FIG 2** Genetic organizations and verification of the PRF-A/FOR-A and COF (and COF-related) gene clusters. (A) Genetic organizations of the PRF-A/FOR-A and COF (and COF-related) gene clusters. The PRF-A gene cluster (*prf*) is from *S. candidus* NRRL 3601, and the FOR-A and COF gene cluster (*foc*) is from *Nocardia interformae* ATCC 21072. The genes responsible for FOR-A and COF biosynthesis (*for* and *cof*) in *S. kaniharaensis* ATCC 21070 are also designated *cof1* to *cof30* (from left to right) (GenBank accession number KY705052). The designation "cof" was used for consistency with the study by Wang et al. (but *cof25*, *cof26*, *cof29*, and *cof30* were missed or not denoted in that work) (17). For the related genes for COF (potential COF) biosynthesis in the other two strains, Arabic numerals (*prf1* to *prf5* and *foc1* to *foc5*) were used for the designations. In addition, the *foc* genes at the top correspond to the *prf* genes, by which the encoded enzymes are homologous. "Late steps for PRF-A/FOR-A" indicates the enzymatic steps after C-glycosidic bond formation during PRF-A/FOR-A biosynthesis. The genes coding for homologous enzymes in these three gene clusters are correspondingly marked by a dotted line. Taking *prfT* (from *S. candidus* NRRL 3601), *focT* (from *Nocardia interformae* ATCC 21072), and *forT* (from *S. kaniharaensis* ATCC 21070) as examples, the enzymes encoded by them are interhomologous. (B) Verification of the gene cluster for the biosynthesis of FOR-A and COF in *Nocardia interformae* ATCC 21072. 21072 indicates the metabolites of *Nocardia interformae* ATCC 21072; PC1 indicates the metabolites of *Nocardia interformae* PC1, in which a 1.8-kb region of the *foc* gene cluster was deleted; and Std indicates the authentic standard of FOR-A. (C) MS/MS analysis of COF from the metabolites of *Nocardia interformae* ATCC 21072. "RA" indicates the relative abundance. "Theor mass" indicates the theoretical mass.

chromosomal region, while the counterpart *foc* gene cluster (26 genes) from *Nocardia interformae* ATCC 21072 is ca. 29.4 kb in size (Fig. 2A and Table S1). As anticipated, *in silico* analysis indicated that the genes for FOR-A and COF biosynthesis are linked together, as reported by a recent study (17). Moreover, there are 7 additional genes (*forW*, *forV*, *forO*, *forG*, *cof25*, *cof26*, and *cof29*) in *S. kaniharaensis* ATCC 21070 (Table S1) that are proposed to execute some alternative functions during FOR-A and COF biosynthesis in this strain.

The *prf* gene cluster is composed of 24 genes and occupies a continuous ~27.1-kb chromosomal region of *S. candidus* NRRL 3601 (Fig. 2A). The homologous *prf* and *foc* gene clusters contain several specialized genes (Fig. 2A). Of these genes, *prfF* (encoding a HAD family hydrolase), *prfH* (encoding a cupin domain-containing protein), *prfI* (encoding flavin reductase), and *prfN* (encoding flavin mononucleotide [FMN] reductase) are present only in the *prf* gene cluster (Table 1). Further analysis indicates that the *foc* gene cluster contains the specialized genes *focH* (5-aminoimidazole-4-carboxamide ribonucleotide transformylase) and *focA* (adenylosuccinate synthetase) for the late steps of FOR-A biosynthesis (Table S1). More interestingly, the candidate genes *prf1*,

**TABLE 1** Deduced functions of the open reading frames in the *prf* gene cluster<sup>a</sup>

Protein	No. of aa	Protein function	Homolog, origin	Identity (%), similarity (%)	GenBank accession no.
PrfA	396	MFS transporter	NbrT6, <i>Nocardia terpenica</i>	72, 84	AJO72759
PrfB	476	Adenylosuccinate lyase	Orf67, <i>Nocardia terpenica</i>	81, 89	AJO72760
PrfF	224	HAD family hydrolase	CLW14_2649, <i>Streptomyces</i> sp. strain 75	56, 66	REE32254
PrfH	118	Cupin domain-containing protein	CRH09_08295, <i>Nocardia terpenica</i>	89, 94	ATL66197
PrfT <sup>b</sup>	334	$\beta$ -RFA-P synthase-like enzyme	Orf61, <i>Nocardia terpenica</i>	81, 87	AJO72754
PrfC	343	SAICAR synthetase	Orf62, <i>Nocardia terpenica</i>	76, 84	AJO72755
PrfS	540	Fumarate reductase/succinate dehydrogenase	Orf63, <i>Nocardia terpenica</i>	77, 83	AJO72756
PrfE	329	Putative monooxygenase	Sare_0593, <i>Salinispora arenicola</i> CNS-205	55, 64	ABV96521
PrfD	444	Putative monooxygenase	Orf75, <i>Nocardia terpenica</i>	79, 86	AJO72768
PrfG	288	Transcriptional regulator	NbrR10, <i>Nocardia terpenica</i>	59, 70	AJO72769
PrfR	351	Glycine/D-amino acid oxidase	EV381_1130, <i>Actinopolyspora</i> sp. strain DSM 45956	70, 79	RZU68182
PrfM	413	Phosphoribosylglycinamide synthetase	Orf72, <i>Nocardia terpenica</i>	77, 86	AJO72765
PrfL	390	Saccharopine dehydrogenase	Orf71, <i>Nocardia terpenica</i>	66, 77	AJO72764
PrfK <sup>b</sup>	437	L-Lysine N <sup>6</sup> -monooxygenase	Spb38, <i>Streptomyces</i> sp. strain SoC090715LN-17	42, 58	BAW27702
PrfJ	668	Methionine-tRNA ligase	Spb40, <i>Streptomyces</i> sp. strain SoC090715LN-17	33, 47	BAW27704
Prf1	250	SAICAR synthetase	PenC, <i>S. antibioticus</i>	69, 79	AKA87338
Prf2	233	Short-chain dehydrogenase	PenB, <i>S. antibioticus</i>	66, 79	AKA87339
Prf3	260	Hydrolase	DI270_030585, <i>Microbispora triticiradicis</i>	39, 54	RG01201
Prf4	288	ATP phosphoribosyltransferase	PenA, <i>S. antibioticus</i>	49, 64	AKA87340
PrfU	402	Phthalate 4,5-dioxygenase	Orf68, <i>Nocardia terpenica</i>	79, 89	AJO72761
PrfQ	387	Amidohydrolase	Orf65, <i>Nocardia terpenica</i>	77, 84	AJO72758
Prf5	404	MFS transporter	D5519_24520, <i>Amycolatopsis panacis</i>	85, 92	RJQ80812
PrfI	156	Flavin reductase	C8D87_103611, <i>Lechevalieria atacamensis</i>	72, 79	RAS67272
PrfN	169	FMN reductase	C8D88_10484, <i>Lechevalieria deserti</i>	71, 82	PWK86923

<sup>a</sup>aa, amino acids; MFS, major facilitator superfamily. SAICAR, phosphoribosylaminoimidazole-succinocarboxamide.

<sup>b</sup>Function confirmed *in vitro* in this study.

*prf2*, and *prf4* (corresponding to *foc1*, *foc2*, and *foc4*) (Table 1), whose products are homologous to PenC, PenB, and PenA, respectively, from the PTN pathway, are also present in the *prf* gene cluster. However, more surprisingly, we were unable to identify COF-related compounds, either COF or PTN, from the culture broths of *S. candidus* NRRL 3601 under laboratory fermentation conditions. Moreover, two particular genes, *focF* (which encodes a dehydrogenase) and *focI* (which encodes an aminotransferase), are present only in the FOR-A gene cluster, suggesting that both genes are involved in dedicated enzymatic steps in FOR-A biosynthesis (Table S1).

**ForK/PrfK functions as a lysine N<sup>6</sup>-monooxygenase.** FOR-A and PRF-A feature a distinctive hydrazine moiety (*N-N* bond) (Fig. 1), which is also present in s56-p1 (19). A recent study revealed that *N-N* bond construction is governed by a cascade of two enzymes, Spb38 (lysine N<sup>6</sup>-monooxygenase) and Spb40 (methionine-tRNA ligase) (19) (Table 1 and Fig. 3A). Bioinformatic analysis of the FOR-A/PRF-A gene cluster identified the candidates ForK/PrfK (deduced lysine N<sup>6</sup>-monooxygenase) and ForJ/PrfJ (methionine-tRNA ligase) (Table S1 and Fig. S2A). To determine if ForK/PrfK fulfills the potential role of lysine N<sup>6</sup>-monooxygenase, we overexpressed and purified the protein in *Escherichia coli* (Fig. S2B). As expected, the ForK/PrfK protein is light yellow (Fig. S2C), a characteristic typical of flavoproteins (Fig. S2D). We then tested their enzymatic activity *in vitro* with L-lysine as the substrate and NADPH as a cofactor. As anticipated, LC-MS analysis indicated that the ForK/PrfK reaction mixtures are capable of generating a distinctive [M + H]<sup>+</sup> ion of



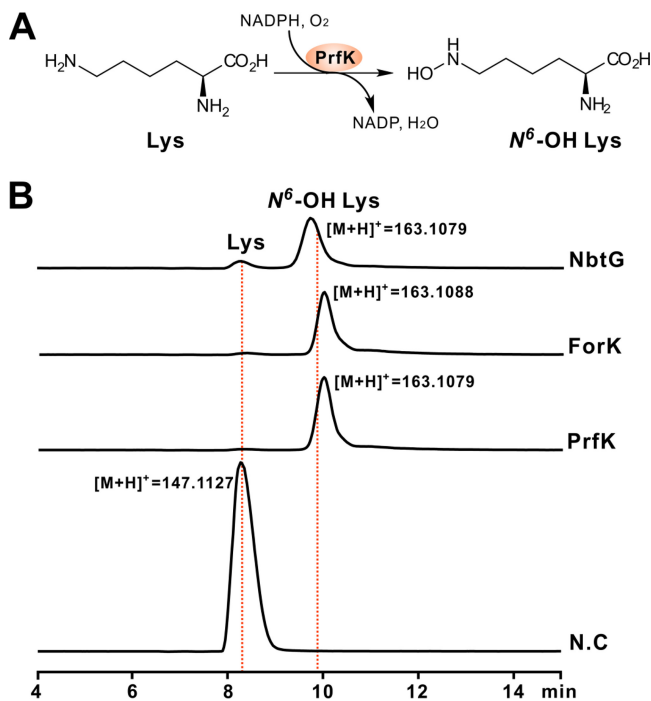


**FIG 3** Biochemical characterization of ForK/PrfK as a lysine (Lys)  $N^6$ -monoxygenase. (A) Scheme of the ForK/PrfK-catalyzed reaction. (B) LC-MS analysis of the ForK/PrfK reaction using lysine as the substrate and NADPH as a cofactor. NbtG indicates the NbtG reaction as a positive control. NbtG (GenBank accession number [BAD55606](#)) is from *Nocardia farcinica* IFM 10152. ForK indicates the ForK reaction, and PrfK indicates the PrfK reaction. N.C, reaction mixture without an enzyme added as a negative control.

$N^6$ -OH lysine (Fig. 3B and Fig. S2E and F), the product of a control reaction with NbtG, a well-characterized lysine  $N^6$ -monoxygenase (Fig. S2G and H) (20).

The negative-control reaction mixtures, without an enzyme added, were unable to produce the expected MS peaks (Fig. 3B). Moreover, we tested the cofactor specificity of the two enzymes, and the LC-MS results indicated that the reaction mixtures with NADH as a cofactor are also able to give the anticipated  $[M + H]^+$  ion of  $N^6$ -OH lysine, confirming that NADH could also support the activity of PrfK/ForK (Fig. S2I). Taken together, these enzymatic data established that PrfK/ForK is a lysine  $N^6$ -monoxygenase likely responsible for the initiation of PRF-A/FOR-A biosynthesis.

**The  $\Delta forT$  and  $\Delta prfT$  mutants accumulate the corresponding intermediates ADCP and DCOP.** FOR-A/PRF-A features an unusual C-nucleoside scaffold, but the biosynthetic construction of the C-C bond has long remained mysterious. *In silico* investigation of the FOR-A/PRF-A gene cluster revealed that *forT* and *prfT* encode a deduced  $\beta$ -RFA-P synthase-like enzyme (Table 1 and Table S1). To investigate the *in vivo* functional role of *forT* and *prfT*, we deleted them in frame using a CRISPR-Cas9 strategy (Fig. S3A to D) (21). As *S. kaniharaensis* ATCC 21070 proved more amenable to in-frame deletion manipulation than *Nocardia interforma* ATCC 21072, it was used in this study for the following genetic experiments. After confirmation by a combined PCR-and-sequencing analysis (Fig. S3A and B), the  $\Delta forT$  mutant was fermented for metabolite analysis. HPLC analysis indicated that this mutant could not generate the distinctive FOR-A peak but was capable of yielding a new peak (4-amino-3,5-dicarboxypyrazole [ADCP]) (Fig. 4A and Fig. S3E to G). LC-MS analysis of ADCP indicates that it shows an apparent  $[M + H]^+$  ion at  $m/z$  172.0353 (Fig. 4A) and a specific fragment ion at  $m/z$  153.8110 (Fig. S3H). Likewise, the confirmed  $\Delta prfT$  mutant (Fig. S3C and D) lacks the capacity for PRF-A and PRF-B production (Fig. S3I and J) but could also generate a new peak (3,5-dicarboxy-4-oxo-4,5-dihydropyrazole [DCOP]) (Fig. 4B and Fig. S3K). LC-MS analysis of the DCOP peak indicates that it shows an apparent  $[M + H]^+$  ion at  $m/z$  173.0193 (Fig. 4B and Fig. S3L).

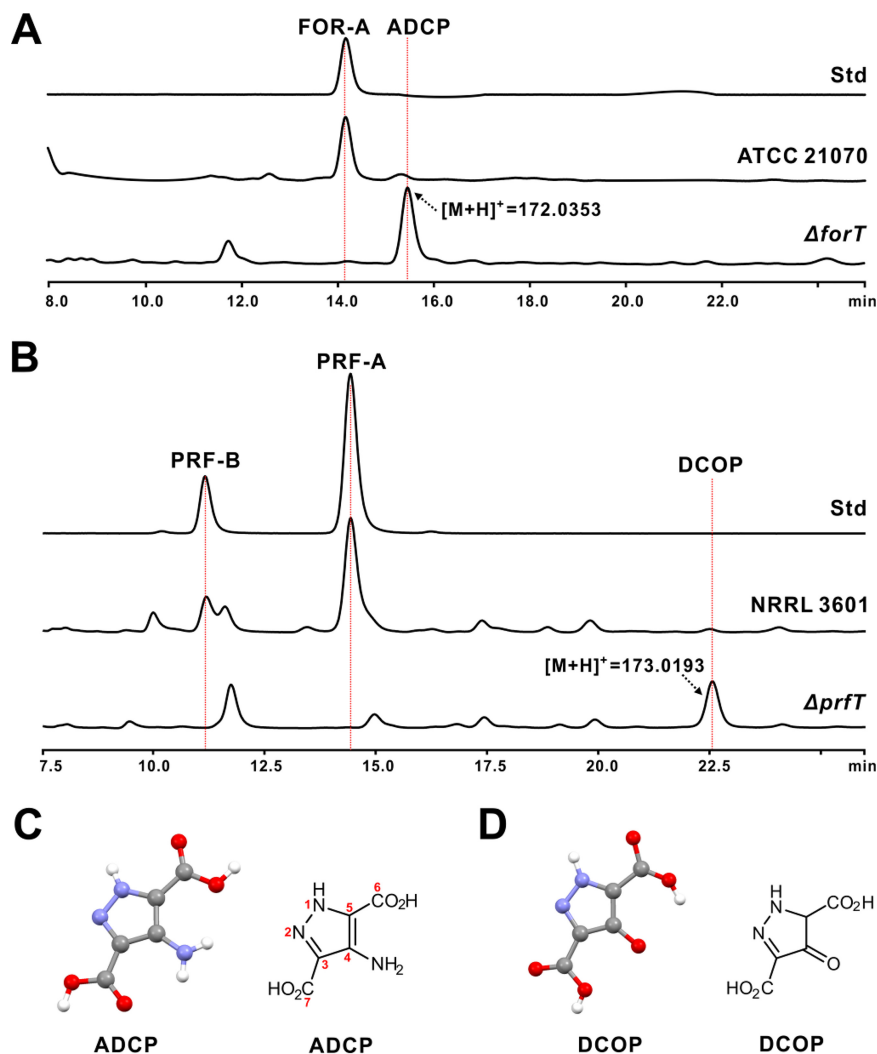


**FIG 4** HPLC analysis of the metabolites produced by the  $\Delta forT$  and  $\Delta prfT$  mutants. (A) HPLC analysis of the metabolites produced by the *S. kaniharaensis*  $\Delta forT$  mutant. Std indicates the authentic standard of FOR-A, ATCC 21070 indicates the metabolites produced by wild-type *S. kaniharaensis* ATCC 21070, and  $\Delta forT$  indicates the metabolites of the  $\Delta forT$  mutant. (B) HPLC traces of the metabolites produced by the *S. candidus*  $\Delta prfT$  mutant. Std indicates the authentic standard of PRF-A, NRRL 3601 indicates the metabolites produced by wild-type *S. candidus* NRRL 3601, and  $\Delta prfT$  indicates the metabolites of the  $\Delta prfT$  mutant. (C) Crystal and chemical structures of ADCP. (D) Crystal and chemical structures of DCOP. The numbering for the atoms of DCOP corresponds to those of ADCP.

To determine the chemical structures of ADCP and DCOP, we initially attempted to purify them via HPLC for nuclear magnetic resonance (NMR) analysis. However, this approach failed to give rise to any apparently detectable  $^1H$  NMR signals for structure elucidation, and we were therefore prompted to optimize the conditions for ADCP/DCOP crystallization for X-ray crystallography determination. This approach showed that ADCP/DCOP harbors a highly conjugated five-membered structural system, in which two *N* atoms (N-1 and N-2) are linked together to form an unusual *N-N* bond (Fig. 4C and D and Table S2). It is this unusual structure of ADCP/DCOP that results in the lack of detectable  $^1H$  signals during NMR analysis. Taken together, the combined genetic and crystallography data suggested that *prfT* and *forT* are most likely the candidate genes for C-C bond formation during PRF-A/FOR-A biosynthesis.

**PrfT/ForT is a  $\beta$ -RFA-P synthase-like enzyme for C-glycosidic bond formation during PRF-A/FOR-A biosynthesis.** Bioinformatic analysis indicated that PrfT/ForT (Table 1 and Table S1) exhibits 81%/64% identities to Orf61 (hypothetic  $\beta$ -RFA-P

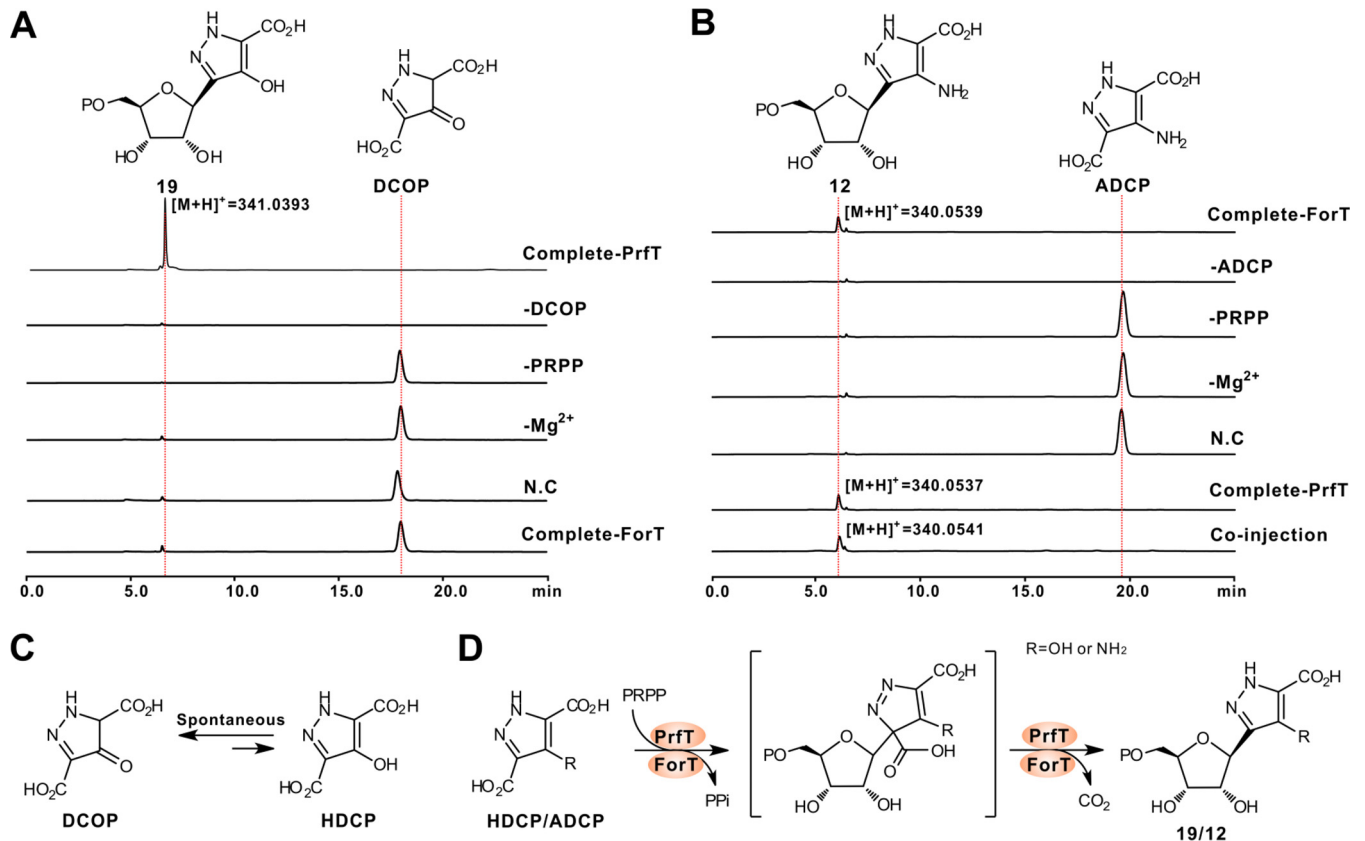


**FIG 5** Biochemical characterization of PrfT and ForT as  $\beta$ -RFA-P synthase-like enzymes for C-glycosidic bond construction. (A) HPLC traces of the PrfT-catalyzed reaction. Complete-PrfT, complete reaction of PrfT with DCOP and PRPP as the substrates; -DCOP, PrfT reaction without DCOP; -PRPP, PrfT reaction without PRPP; -Mg<sup>2+</sup>, PrfT reaction without Mg<sup>2+</sup>; N.C, PrfT reaction lacking an enzyme as the negative control; Complete-ForT, complete reaction of ForT with DCOP and PRPP as the substrate. (B) HPLC traces of the ForT-catalyzed reaction. Complete-ForT, complete reaction of ForT using ADCP and PRPP as the substrates; -ADCP, ForT reaction without ADCP; -PRPP, ForT reaction without PRPP; -Mg<sup>2+</sup>, ForT reaction without Mg<sup>2+</sup>; N.C, ForT reaction without an enzyme as a negative control; Complete-PrfT, complete reaction of PrfT with ADCP and PRPP as the substrates; Co-injection, coinjection of the ForT reaction mixture and the PrfT reaction mixture. (C) Scheme of the tautomerization reaction between DCOP and HDCP (4-hydroxy-3,5-dicarboxypyrazole). (D) Proposed mechanism for the PrfT/ForT-catalyzed reaction. When the R group is OH (NH<sub>2</sub>), the reaction is from HDCP to compound 19 (ADCP to compound 12).

synthase) from *Nocardia terpenica* (Fig. S4A).  $\beta$ -RFA-P synthase is responsible for the first committed step of methanopterin biosynthesis, catalyzing the conversion of phosphoribosyl pyrophosphate (PRPP) and *p*-aminobenzoate to  $\beta$ -RFA-P (Fig. 1) and CO<sub>2</sub> (22). To obtain direct biochemical evidence that PrfT/ForT governs C-glycosidic bond construction during PRF-A/FOR-A biosynthesis, we overexpressed and purified these proteins from *E. coli* to near homogeneity and assayed them *in vitro* using PRPP and DCOP/ADCP as the substrates (Fig. S4B and C). The HPLC traces indicated that the product of the PrfT reaction is capable of producing a new peak, which is absent from that of the negative control (the reaction mixture without PrfT added) (Fig. 5A, C, and D and Fig. S4D). Further LC-MS analysis indicated that the product of the PrfT reaction exhibits an obvious [M + H]<sup>+</sup> ion at *m/z* 341.0393 (Fig. 5A and Fig. S4E and F). Moreover, the reaction mixture without the divalent metal Mg<sup>2+</sup> is not able to generate the characteristic peak of the product. We therefore purified the target compound for further <sup>1</sup>H, <sup>13</sup>C, and two-dimensional (2D) NMR analyses (Fig. S5 and Table S3), and its chemical structure, on the basis of the combined NMR and tandem MS (MS/MS) analyses, was finally determined as compound 19.

Similarly, the ForT reaction mixtures, as analyzed by HPLC analysis, are also capable of producing a novel characteristic peak (compound 12) (Fig. 5B and Fig. S4G), which is distinctly absent from the reaction mixtures without ForT/Mg<sup>2+</sup>. Additional MS/MS analyses showed that the target peak could produce an apparent [M + H]<sup>+</sup> ion at *m/z* 340.0539 (Fig. 5B), with major fragment ions completely consistent with the theoretical



fragmentation pattern of compound 12 (Fig. S4H and I). We then tested the substrate flexibility of PrfT for these compounds, and the results indicated that this enzyme could accept ADCP to form compound 12 (Fig. 5B and Fig. S4J to M) but that, conversely, ForT is not capable of recognizing DCOP as the substrate (Fig. 5A).

Subsequently, we examined the specificities of divalent metal ions for PrfT/ForT activity. Of the 6 divalent metal ions selected,  $Mn^{2+}$  and  $Co^{2+}$  are able to maintain maximal activity for PrfT (100%), but this indicates either dramatically decreased activity in the presence of  $Ni^{2+}/Zn^{2+}$  or negative activity with  $Ca^{2+}/Cu^{2+}$  added instead (Fig. S4N). For the ForT reaction,  $Co^{2+}$  could also support its maximal activity, while  $Mn^{2+}$  (61%),  $Ni^{2+}$  (52%),  $Zn^{2+}$  (84%), or  $Ca^{2+}/Cu^{2+}$  (0%) is just partially able or unable to replace  $Mg^{2+}$  to support the enzymatic activity of ForT (Fig. S4O). All of these biochemical data demonstrate that PrfT/ForT functions as an unusual  $\beta$ -RFA-P synthase-like enzyme for C-glycosidic bond formation during PRF-A/FOR-A biosynthesis.

## DISCUSSION

Previous metabolic labeling experiments determined that glutamate and lysine were the precursors for FOR-A and PRF-A biosynthesis and that the ribosyl moiety of both antibiotics was obtained directly from primary metabolism (15, 16). In the present study, this assignment is shown to be essentially correct. Insight into the biosynthetic gene cluster of PRF-A/FOR-A (only the PRF enzymes for common steps of both antibiotics are listed in Fig. 6) resulted in the identification of the enzymes for the construction of the pyrazole ring system (Fig. 6A). PRF-A biosynthesis is proposed to be initiated by PrfK hydroxylating L-lysine to form  $N^6$ -OH lysine (compound 1), which, in common with most lysine  $N^6$ -monooxygenases, prefers NADPH as a cofactor (20). Subsequently, compound 1 and L-glutamate are utilized by PrfJ (methionine-tRNA ligase) to construct the N-N bond of compound 2. PrfR (amino acid oxidase) then catalyzes the reaction to afford compound 3 (with leaving of compound 4), which is subsequently dehydrogenated by PrfS to form compound 5. From this, we tentatively propose that compound 5 is hydroxylated by PrfE/D in a sequential manner at the C-4 position to generate compound 6, which would be successively dehydrated either spontaneously or via an unknown enzymatic strategy to give rise to compound 7. Further investigation of the PRF-A gene cluster resulted in the identification of a candidate enzyme, PrfM (phosphoribosyl-glycinamide synthetase-like protein), which usually catalyzes the second step in the *de novo* purine pathway (23). We therefore postulate that compound 7, under the catalysis of PrfM, is subsequently converted to compound 8 for the completion of pyrazole ring construction. Thereafter, we propose that compound 8, after oxidation to DCOP (compound 9a), will undergo further sequential reactions to complete PRF-A biosynthesis (Fig. 6A).

As for FOR-A biosynthesis, we deduce that DCOP acts as a potential amino group acceptor and is modified by the aminotransferase ForI to compound 10, which is then dehydrogenated to give ADCP (compound 11). Actually, these particular enzymes, the aminotransferase (ForI) and dehydrogenase (ForF), are absent from the PRF-A pathway, implying that they should perform these definite functions to accomplish ADCP biosynthesis (Fig. 6A), and related biochemical studies in our laboratory are now ongoing. Once the C-glycosidic bond is constructed, the late enzymatic steps are highly similar to those in the *de novo* purine pathway, which has already been illustrated in two recent studies (17, 24).

There are several other genes (*prfHLIN*) whose functional roles are still ambiguous. In particular, the product of *prfH* (cupin domain-containing protein) is probably responsible for the conversion of PRF-B to PRF-A, although it is also possible for this reaction to occur spontaneously. Hence, PrfH is tentatively proposed to be an isomerase during PRF-A biosynthesis, and PrfL is a potential saccharopine dehydrogenase, which normally plays a key role in lysine biosynthesis (25). Accordingly, we propose that PrfL could be responsible for a salvage pathway for lysine regeneration during PRF-A biosynthesis (Fig. 6B). The two remaining proteins, PrfI and PrfN, are apparently

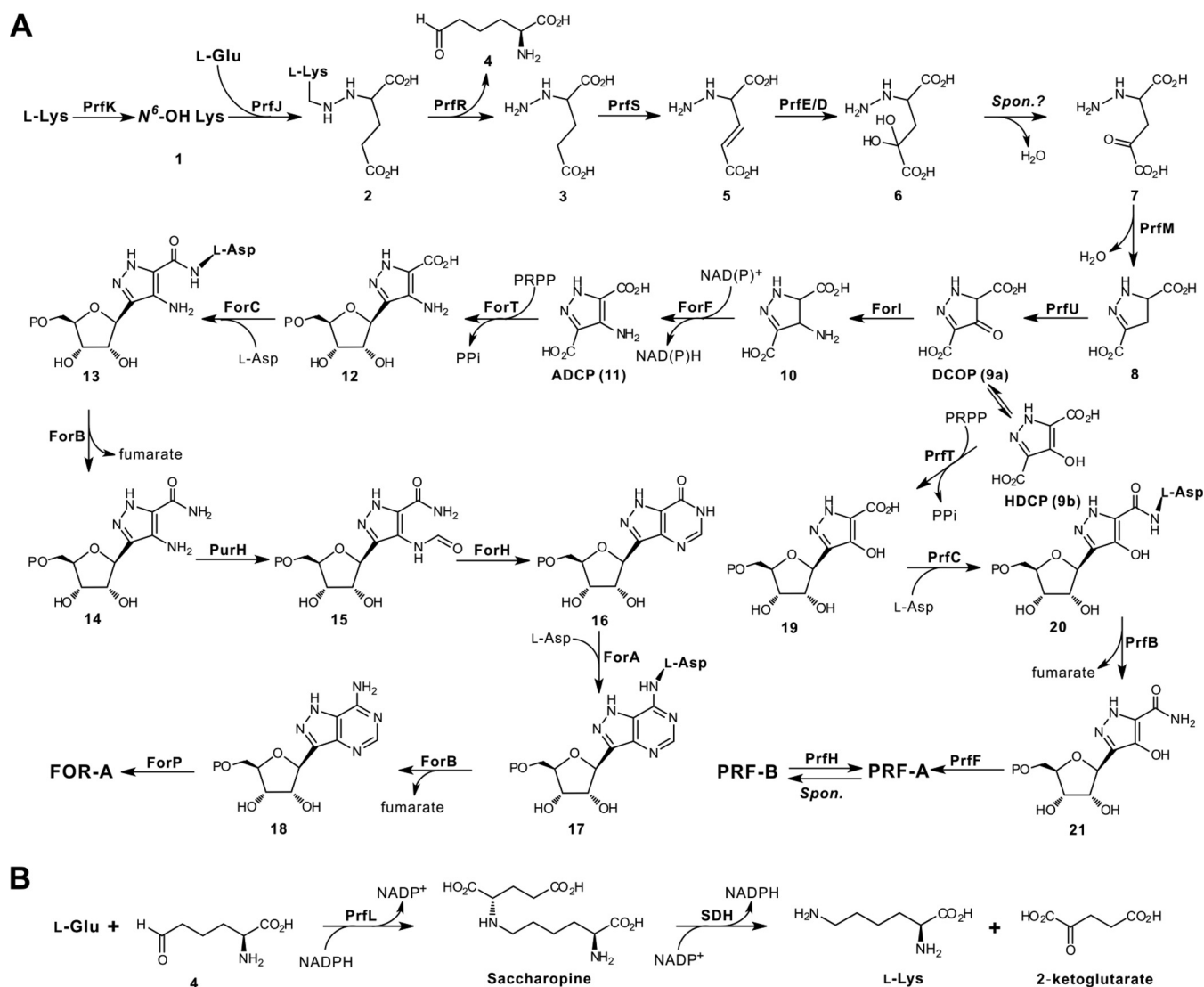


**FIG 6** Proposed biosynthetic pathways to FOR-A and PRF-A. (A) Proposed pathways to FOR-A and PRF-A. We propose that they share identical steps at the early stage prior to the construction of C-nucleoside scaffolds. HDCP, 4-hydroxy-3,5-dicarboxypyrazole. (B) Proposed salvage pathway for the regeneration of lysine during FOR-A/PRF-A biosynthesis. SDH, short-chain dehydrogenase, which is from the primary metabolic pathway for lysine regeneration. *Spon.*, spontaneous.

homologous to flavin/FMN reductase and could be involved in the reductive recycling of the FMN/flavin adenine dinucleotide (FAD) cofactor in PRF-A biosynthesis.

C-Nucleoside antibiotics have increasingly gained interest for clinical uses in the past decades (2), but their biosynthetic logics have long been underappreciated due to their difficult-to-access pathways. Indeed, nature has developed several diverse strategies for C-glycosidic bond construction during the biosynthesis of this group of antibiotics. Showdomycin biosynthesis uses a YeiN-like C-glycosyltransferase to build the C-C bond (3), while the biosynthesis of pseudouridimycin and malayamycin exploits a tRNA pseudouridylate synthase (TruD-like) for C-glycosidic bond construction (4, 26). In the present study, FOR-A and PRF-A are shown to harness a totally different  $\beta$ -RFA-P synthase-like enzyme (ForT/PrfT) to catalyze the formation of C-glycosides (Fig. 6A). The usual role for  $\beta$ -RFA-P synthase has exclusively been in the biosynthesis of the modified folate methanopterin (22). In this respect, ForT/PrfT represents an example of this kind of enzyme responsible for C-glycosidic bond formation in natural product biosynthesis. Hence, similar to  $\beta$ -RFA-P synthase (22), we predict that ForT/PrfT should employ an  $S_N1$ -like enzymatic strategy associated with cryptic decarboxylation for the construction of the C-glycosidic bond. Notably, the single  $\beta$ -RFA-P synthase-like enzyme (ForT/

**TABLE 2** Strains and plasmids used in this study

Strain or plasmid	Relevant characteristic(s)	Source or reference
<b>Strains</b>		
<i>Nocardia interforma</i> ATCC 21072	Wild-type FOR-A producer	ATCC
<i>S. kaniharaensis</i> ATCC 21070	Wild-type FOR-A producer	ATCC
<i>S. resistomycificus</i> NRRL 2290	New FOR-A producer	NRRL
<i>Salinispora arenicola</i> CNS-205	Potential FOR-A producer	29
<i>S. candidus</i> NRRL 3601	Wild-type PRF-A producer	NRRL
<i>Nocardia interforma</i> PC1	ATCC 21072 derivative with deletion of a 1.8-kb region (containing <i>focI</i> , <i>foc1</i> , and <i>foc2</i> )	This study
<i>S. kaniharaensis</i> $\Delta$ <i>forT</i>	ATCC 21070 derivative with in-frame deletion of <i>forT</i>	This study
<i>S. candidus</i> $\Delta$ <i>prfT</i>	NRRL 3601 derivative with in-frame deletion of <i>prfT</i>	This study
<i>E. coli</i> DH10B	F <sup>-</sup> <i>mcrA</i> $\Delta$ ( <i>mrr-hsdRMS-mcrBC</i> ) $\phi$ 80 <i>dlacZ</i> $\Delta$ M15 $\Delta$ <i>lacX74</i> <i>deoR recA1 endA1 araD139</i> $\Delta$ ( <i>ara leu</i> )7697 <i>galU galK</i> $\lambda^-$ <i>rpsL nupG</i>	Gibco-BRL
<i>E. coli</i> Rosetta(DE3)/pLysS	F <sup>-</sup> <i>ompT hsdS<sub>B</sub></i> (r <sub>B</sub> <sup>-</sup> m <sub>B</sub> <sup>-</sup> ) <i>gal dcm</i> $\lambda$ (DE3 [ <i>lacI lacUV5-T7</i> gene 1 <i>ind1 sam7 nin5</i> ]) pLysS(Cml <sup>r</sup> )	Novagen
<i>E. coli</i> ET12567(pUZ8002)	ET12567 containing helper plasmid pUZ8002	28
<b>Plasmids</b>		
pEASY-Blunt	pUCori <i>lacZ f1 ori</i> ; Kan Amp	TransGen Biotech
pET28a	<i>neo rep<sup>PMB1</sup></i> ; T7 promoter	Novagen
pET28a/ <i>forT</i>	pET28a derivative carrying an NdeI-EcoRI fragment containing <i>forT</i>	This study
pET28a/ <i>forK</i>	pET28a derivative carrying an NdeI-EcoRI fragment containing <i>forK</i>	This study
pET28a/ <i>prfT</i>	pET28a derivative carrying an NdeI-EcoRI fragment containing <i>prfT</i>	This study
pET28a/ <i>prfK</i>	pET28a derivative carrying an NdeI-EcoRI fragment containing <i>prfK</i>	This study
pET28a/ <i>nbtG</i>	pET28a derivative carrying an NdeI-EcoRI fragment containing <i>nbtG</i>	This study
pCHW351	pOJ446 derivative carrying a 2.8-kb XbaI-BglII left arm, a 2.9-kb BglII blunt right arm, and <i>tsr</i> for the replacement of <i>focI</i> , <i>foc1</i> , and <i>foc2</i>	This study
pCHW352	pCRISPR-Cas9 derivative carrying an XbaI-NcoI gRNA, a 2.0-kb left arm, and a 1.8-kb right arm for in-frame deletion of <i>forT</i>	This study
pCHW353	pCRISPR-Cas9 derivative carrying an XbaI-NcoI gRNA, a 1.8-kb left arm, and a 2.2-kb right arm for in-frame deletion of <i>prfT</i>	This study

PrfT) could be used as a promising probe for the rational mining of related C-nucleoside antibiotics, and we have already discovered several potential PRF-A/FOR-A group antibiotic pathways from the currently available reservoir of microbial genomes (see Fig. S6 in the supplemental material).

In summary, we report the pathways for FOR-A and PRF-A biosynthesis using a genomics-led approach and have delineated the associated FOR-A gene cluster diversity in actinobacteria. We also propose that the biosynthesis of FOR-A and PRF-A is likely initiated by a lysine N<sup>6</sup>-monooxygenase and show that PrfT/ForT adopts a unique strategy for C-glycosidic bond formation in nucleoside antibiotic biosynthesis. We anticipate that the C-glycosyltransferases shown in this study may serve as an inspiration for future catalyst design to generate analogs of potential therapeutic value.

## MATERIALS AND METHODS

**General materials and methods.** Strains and plasmids used in this study are listed in Table 2, and primers are listed in Table 3. General methods employed in this work were performed according to standard protocols described previously by Green and Sambrook (27) or Kieser et al. (28).

**Enzymes, chemicals, and reagents.** All of the enzymes used in this study were purchased from New England Biolabs. The chemicals and reagents were products of Sigma-Aldrich, Thermo Scientific, or J&K Scientific. The standards of FOR-A and PRF were individual products of Biorbyt and Sigma-Aldrich.

**Sequencing analysis of *S. kaniharaensis* ATCC 21070, *Nocardia interforma* ATCC 21072, and *S. candidus* NRRL 3601.** Sequencing of the genomes of *S. kaniharaensis* ATCC 21070, *Nocardia interforma* ATCC 21072, and *S. candidus* NRRL 3601 was performed on an Illumina HiSeq 2500 system machine. The

**TABLE 3** PCR primers used in this study

Primer	Sequence (5'-3')
Ni-lfdsaicar-LF	GGTGGCGGTCAACAACGA
Ni-lfdsaicar-LR	GGTGGCGACGAAGAATCA
Ni-lfdsaicar-RF	GTCCATATGGCACTTGACCGACCC
Ni-lfdsaicar-RR	GGAATTCAGGAGACGACGGTGGT
LfdsaicarF	GTCCATATGCCGGAGACTTTCGAT
LfdsaicarR	GGAATTCAGCGCCCCGTGTTGAG
forT-cas9-gRNA-F	GATGGGTCAACGAGATCACCTTCACGTTTTAGAG
forT-cas9-gRNA-R	CTAGCTCTAAAACGTGAAGGTGATCTCGTTGACC
forT-cas9-LF	TCGTGCAAGGCACTAGAAGGCCAGCGGCAGCACGACCTTT
forT-cas9-LR	TCAGGAGACGACGGTGGTGGCGTCGGGTCAAGTGCCAT
forT-cas9-RF	GCCACCACCGTCGCTCCTGA
forT-cas9-RR	GGTCGATCCCGCATATAGGCGGTGACGAGTCCAGGTAGCC
forT-cas9-idF	AACTTCCAGCCGTGGTAGATGC
forT-cas9-idR	CGGTCTTCATTGCCCTGCTTT
prfT-cas9-gRNA-F	GATGGGTCAACGAGCTGACCTTCACGTTTTAGAG
prfT-cas9-gRNA-R	CTAGCTCTAAAACGTGAAGGTGACGCTCGTTGACC
prfT-cas9-LF	TCGTGCAAGGCACTAGAAGGACGAGAAGTCCGCACCAG
prfT-cas9-LR	TGTTGCGGACCGTGGTGAAGGATTCGCCGTCGAGGCT
prfT-cas9-RF	TTCACCACGGTCCGCAACA
prfT-cas9-RR	GGTCGATCCCGCATATAGGCAACGGGTATCGGTTGACG
prfT-cas9-idF	AAGGCGGAGTTCGGGTTC
prfT-cas9-idR	CGTGTTCATCGACTGGGAGA
forT-28a-exp-F	GCTTAGAACCCGACTACGGACAGGACC
forT-28a-exp-R	GAAGATCTGTAGCCGATGCGGAACGAG
forK-28a-exp-F	GAAGATCTGGAGGAGCGGAACACG
forK-28a-exp-R	GGAATTCACGCGGAAGACCACATCG
prfT-28a-exp-F	GTCCATATGACGGGAACCGCGGTG
prfT-28a-exp-R	GGAATTCCTACAGCCAGGTGCGGGC
prfK-28a-exp-F	GTCCATATGAGCACCGGACACGAC
prfK-28a-exp-R	GGAATTCAGAACGTCAGCGCGAC

raw data were processed to render the resulting clean reads, which were assembled by using Velvet software (v1.2.07) to obtain the scaffold. Detailed methods and programs used for genome annotations and accurate bioinformatic analysis were performed according to protocols described previously by Xu et al. (18).

**Fermentation and detection of related nucleoside antibiotics.** *S. kaniharaensis* ATCC 21070, *Nocardia interforma* ATCC 21072, and *S. candidus* NRRL 3601 were cultivated on YS agar (2 g yeast extract, 10 g soluble starch, and 15 g agar per liter [pH 7.3]). For fermentation, a single clone was inoculated in tryptic soy broth (TSB) and cultivated for 2 days; after that, the cultures (2%, vol/vol) were transferred to fermentation medium (16) and fermented (180 rpm at 28°C) for 7 days. For HPLC and LC-MS analyses, the fermentation beer was processed by adding oxalic acid until pH 3.0 was reached. HPLC analysis was performed using a Shimadzu LC-20AT instrument equipped with a C<sub>18</sub> column (5 μm, 4.6 by 250 mm; Shimadzu), with an elution gradient of 10% to 30% methanol–0.15% aqueous TFA (trifluoroacetic acid) over 30 min at a flow rate of 0.5 ml/min. LC-MS analysis was carried out on a Thermo Fisher Scientific ESI-LTQ Orbitrap instrument controlled by Xcalibur in the positive mode. The parameters for MS analysis are as follows: a capillary temperature of 275°C and a capillary voltage of 35 V.

**Construction of the *Nocardia interforma* PC1, *S. kaniharaensis* Δ*forT*, and *S. candidus* Δ*prfT* mutants.** For the construction of the mutant strain *Nocardia interforma* PC1, a strategy similar to the one described previously by Wu et al. (9), with Ni-lfdsaicar-LF/R (left arm) and Ni-lfdsaicar-RF/R (right arm) as primers and pOJ446 as the starter vector, was also used in this study. For the construction of the *S. kaniharaensis* Δ*forT* mutant (taking it as an example), pCHW352 (Table 2) was generated, using methods similar to the ones described previously by Mo et al. (21), and then introduced into *S. kaniharaensis* via conjugation. After confirmation, the conjugant, induced by thiostrepton, was screened and verified on the basis of standard methods (28). Likewise, the *S. candidus* Δ*prfT* mutant was constructed according to the protocols described above.

**Overexpression and purification of the target proteins.** Synthesis of *nbtG* (whose sequence was optimized based on *E. coli* codon preference; GenBank accession number [MN370059](#)) was conducted by Synbio Tech, using pET28a as the expression vector. Expression and purification of NbtG, Fork, ForT, PrfK, and PrfT were carried out in a way similar to the one described previously by Wu et al. (9). After concentration, the purified proteins were buffer exchanged into the stock buffer (25 mM Tris, 150 mM NaCl, and 10% glycerol [pH 7.5 for Fork, ForT, PrfK, and PrfT and pH 8.0 for NbtG]) using Amicon Ultra filters. Finally, the purified proteins were flash-frozen in liquid nitrogen and stored at –80°C.

**In vitro assays of NbtG, Fork, and PrfK.** Reaction mixtures (100 μl each) consisted of a solution containing 50 mM potassium phosphate buffer (pH 7.5), 1 mM L-lysine, 1 mM NAD(P)H, and 20 μg NbtG, Fork, or PrfK at 30°C. Reactions were terminated after 4 h by the addition of an equivalent volume (100 μl) of methanol. Following centrifugation to remove the protein, the reactions were analyzed by

using an LC-HRMS system equipped with a reverse-phase  $C_{18}$  column with 0.15% TFA (95%)–methanol (5%) at a flow rate of 0.4 ml/min for 20 min. The parameters for MS analysis are the same as the ones described above.

**In vitro assays of ForT and PrfT.** Reaction mixtures (100  $\mu$ l each) consisting of 50 mM Tris-Cl buffer (pH 8.0), 1.5 mM PRPP, 20 mM  $Mg^{2+}$  (or other related divalent metal ions), 1 mM ADCP/DCOP, and 20  $\mu$ g ForT/PrfT were incubated at 30°C for 4 h. After that, reactions were terminated by the addition of an equivalent volume (100  $\mu$ l) of methanol, and protein was removed by centrifugation. The HPLC analysis was performed on a reverse-phase  $C_{18}$  column (5  $\mu$ m, 4.6 by 250 mm; Shimadzu) with an elution gradient of 10% to 30% methanol–0.1% aqueous TFA (HPLC grade) over 15 min at 0.5 ml/min, the methanol system was then returned to the initial 10%, and the ratio was maintained for another 15 min. Elution was monitored at 290 nm (for the ForT reaction) or 270 nm (for the PrfT reaction) with a diode array detector (DAD), and the data were analyzed offline with Shimadzu data software.

**Isolation and purification of the target metabolites ADCP and DCOP.** For the isolation of ADCP and DCOP, the fermentation beers (7 day) of mutant strains (*S. kaniharaensis*  $\Delta$ forT and *S. candidus*  $\Delta$ prfT) were processed by adding oxalic acid until pH 3.0 was reached and centrifuged at 6,000 rpm for 15 min. The supernatant was collected and then extracted three times with an equal volume of *n*-butanol. The collected extract (upper layer) was condensed and further dried by rotary evaporation and lyophilization, and the dried residues were then redissolved in 50% methanol and passed through a  $C_{18}$  solid-phase extraction cartridge. Finally, approximately 100 mg of the compound ADCP/DCOP could be isolated and purified from 10 liters of fermentation beers by preparative HPLC (the HPLC conditions are identical to those described above but with a flow rate of 5 ml/min).

For the purification of compound 19, the PrfT reaction (4 h) was terminated, and the reaction mixtures (100 ml) were then collected and passed through Dowex 50WX8 ( $H^+$ ) resin (the ratio of the reaction mixtures to resin is 3:1). The flowthrough liquid was collected and condensed. After that, about 4 mg of compound 19 was prepared by HPLC with a flow rate of 0.4 ml/min (5% methanol–0.2% aqueous TFA) over 15 min.

**Single-crystal X-ray diffraction for ADCP and DCOP.** For growth of crystals of ADCP and DCOP, the solvent system (the ratio of water to methanol is 1:1) was selected to dissolve adequate ADCP and DCOP to a near-saturated state. The bottle of the sample vial was sealed by Parafilm with sporadically distributed pores. After leaving it at 4°C for about 2 weeks, needle-like crystals of ADCP and square-like crystals of DCOP appeared due to the easier evaporation of methanol and lower solubility of the compound in water. The crystals of the target compound were determined using a Bruker Apex Duo single-crystal X-ray diffractometer, and the related data, including space groups, crystal molecular structures, and intermolecular hydrogen bonds, etc., are listed in Table S2 in the supplemental material. The individual CCDC numbers for DCOP and ADCP are 1947450 and 1947811.

**NMR analysis of compound 19.** NMR spectra of compound 19 were recorded on an Agilent DD2 600-MHz NMR spectrometer, using  $D_2O$  as the solvent.

**Accession number(s).** The DNA sequences have been deposited in the GenBank database under accession numbers [KY705052](#) (for the FOR-A and COF gene clusters from *S. kaniharaensis* ATCC 21070), [MH493900](#) (for the PRF gene cluster from *S. candidus* NRRL 3601), and [KY682079](#) (for the FOR-A and COF gene clusters from *Nocardia interforma* ATCC 21072), as well as [MN370059](#).

## SUPPLEMENTAL MATERIAL

Supplemental material is available online only.

**SUPPLEMENTAL FILE 1**, PDF file, 3.7 MB.

## ACKNOWLEDGMENTS

We are grateful to Paul R. Jensen from UCSD (CA, USA) for kindly providing us with *Salinispora arenicola* strain CNS-205. We also sincerely thank Pablo Sobrado from Virginia Tech (VA, USA) for the generous gift of the NbtG expression plasmid.

This work was supported by grants from the National Key R&D Program of China (2018YFA0903203) and the National Natural Science Foundation of China (31770041 and 31970052).

## REFERENCES

1. Isono K. 1988. Nucleoside antibiotics: structure, biological activity, and biosynthesis. *J Antibiot (Tokyo)* 41:1711–1739. <https://doi.org/10.7164/antibiotics.41.1711>.
2. De Clercq E. 2016. C-nucleosides to be revisited. *J Med Chem* 59: 2301–2311. <https://doi.org/10.1021/acs.jmedchem.5b01157>.
3. Palmu K, Rosenqvist P, Thapa K, Iliina Y, Siitonen V, Baral B, Mäkinen J, Belogurov G, Virta P, Niemi J, Metsä-Ketelä M. 2017. Discovery of the showdomycin gene cluster from *Streptomyces showdoensis* ATCC 15227 yields insight into the biosynthetic logic of C-nucleoside antibiotics. *ACS Chem Biol* 12:1472–1477. <https://doi.org/10.1021/acschembio.7b00078>.
4. Sosio M, Gaspari E, Iorio M, Pessina S, Medema MH, Bernasconi A, Simone M, Maffioli SI, Ebricht RH, Donadio S. 2018. Analysis of the pseudouridimycin biosynthetic pathway provides insights into the formation of C-nucleoside antibiotics. *Cell Chem Biol* 25:540–549. <https://doi.org/10.1016/j.chembiol.2018.02.008>.
5. Hori M, Takita T, Koyama G, Tadeuchi T, Umezawa H. 1964. A new antibiotic, formycin. *J Antibiot (Tokyo)* 17:96–99.
6. Aizawa S, Hidaka T, Ōtake N, Yonehara H, Isono K, Igarashi N, Suzuki S. 1965. Studies on a new antibiotic, Laurusin. *Agr Biol Chem* 29:375–376. <https://doi.org/10.1080/00021369.1965.10858402>.



7. Ishizuka M, Sawa T, Hori S, Takayama H, Takeuchi T. 1968. Biological studies on formycin and formycin B. *J Antibiot (Tokyo)* 21:5–12. <https://doi.org/10.7164/antibiotics.21.5>.
8. Nakamura H, Koyama G, Iitaka Y, Ono M, Yagiawa N. 1974. Structure of coformycin, an unusual nucleoside of microbial origin. *J Am Chem Soc* 96:4327–4378. <https://doi.org/10.1021/ja00820a049>.
9. Wu P, Wan D, Xu G, Wang G, Ma H, Wang T, Gao Y, Qi J, Chen X, Zhu J, Li YQ, Deng Z, Chen W. 2017. An unusual protector-protége strategy for the biosynthesis of purine nucleoside antibiotics. *Cell Chem Biol* 24:171–181. <https://doi.org/10.1016/j.chembiol.2016.12.012>.
10. Gao Y, Xu G, Wu P, Liu J, Cai YS, Deng Z, Chen W. 2017. Biosynthesis of 2'-chloropentostatin and 2'-amino-2'-deoxyadenosine highlights a single gene cluster responsible for two independent pathways in *Actinomadura* sp. strain ATCC 39365. *Appl Environ Microbiol* 83:e00078-17. <https://doi.org/10.1128/AEM.00078-17>.
11. Xia Y, Luo F, Shang Y, Chen P, Lu Y, Wang C. 2017. Fungal cordycepin biosynthesis is coupled with the production of the safeguard molecule pentostatin. *Cell Chem Biol* 24:1479–1489. <https://doi.org/10.1016/j.chembiol.2017.09.001>.
12. Gutowski GE, Sweeney MJ, DeLong DC, Hamill RL, Gerzon K, Dyke RW. 1975. Biochemistry and biological effects of the pyrazofurins (pyrazomycins): initial clinical trial. *Ann N Y Acad Sci* 255:544–551. <https://doi.org/10.1111/j.1749-6632.1975.tb29257.x>.
13. Cadman E, Benz C. 1980. Uridine and cytidine metabolism following inhibition of *de novo* pyrimidine synthesis by pyrazofurin. *Biochim Biophys Acta* 609:372–382. [https://doi.org/10.1016/0005-2787\(80\)90111-2](https://doi.org/10.1016/0005-2787(80)90111-2).
14. Worzalla JF, Sweeney MJ. 1980. Pyrazofurin inhibition of purine biosynthesis via 5-aminoimidazole-4-carboxamide-1-beta-D-ribofuranosyl 5'-monophosphate formyltransferase. *Cancer Res* 40:1482–1485.
15. Buchanan JG, Hamblin MR, Sood GR, Wightman RH. 1980. The biosynthesis of pyrazofurin and formycin. *J Chem Soc Chem Commun* 19:917–918. <https://doi.org/10.1039/c39800000917>.
16. Ochi K, Yashima S, Eguchi Y, Matsushita K. 1979. Biosynthesis of formycin-incorporation and distribution of C-13, C-14, and N-15-labeled compounds into formycin. *J Biol Chem* 254:8819–8824.
17. Wang SA, Ko Y, Zeng J, Geng Y, Ren D, Ogasawara Y, Irani S, Zhang Y, Liu HW. 2019. Identification of the formycin A biosynthetic gene cluster from *Streptomyces kaniharaensis* illustrates the interplay between biological pyrazolopyrimidine formation and *de novo* purine biosynthesis. *J Am Chem Soc* 141:6127–6131. <https://doi.org/10.1021/jacs.9b00241>.
18. Xu G, Kong L, Gong R, Xu L, Gao Y, Jiang M, Cai YS, Hong K, Hu Y, Liu P, Deng Z, Price NPJ, Chen W. 2018. Coordinated biosynthesis of the purine nucleoside antibiotics aristeromycin and coformycin in actinomycetes. *Appl Environ Microbiol* 84:e01860-18. <https://doi.org/10.1128/AEM.01860-18>.
19. Matsuda K, Tomita T, Shin-Ya K, Wakimoto T, Kuzuyama T, Nishiyama M. 2018. Discovery of unprecedented hydrazine-forming machinery in bacteria. *J Am Chem Soc* 140:9083–9086. <https://doi.org/10.1021/jacs.8b05354>.
20. Binda C, Robinson RM, Martin Del Campo JS, Keul ND, Rodriguez PJ, Robinson HH, Mattevi A, Sobrado P. 2015. An unprecedented NADPH domain conformation in lysine monooxygenase NbtG provides insights into uncoupling of oxygen consumption from substrate hydroxylation. *J Biol Chem* 290:12676–12688. <https://doi.org/10.1074/jbc.M114.629485>.
21. Mo J, Wang S, Zhang W, Li C, Deng Z, Zhang L, Qu X. 2019. Efficient editing DNA regions with high sequence identity in actinomycetal genomes by a CRISPR-Cas9 system. *Synth Syst Biotechnol* 4:86–91. <https://doi.org/10.1016/j.synbio.2019.02.004>.
22. Rasche ME, White RH. 1998. Mechanism for the enzymatic formation of 4-(beta-D-ribofuranosyl)aminobenzene 5'-phosphate during the biosynthesis of methanopterin. *Biochemistry* 37:11343–11351. <https://doi.org/10.1021/bi973086q>.
23. Sampei G, Baba S, Kanagawa M, Yanai H, Ishii T, Kawai H, Fukai Y, Ebihara A, Nakagawa N, Kawai G. 2010. Crystal structures of glycinamide ribonucleotide synthetase, PurD, from thermophilic eubacteria. *J Biochem* 148:429–438. <https://doi.org/10.1093/jb/mvq088>.
24. Ko Y, Wang SA, Ogasawara Y, Ruszczycky MW, Liu HW. 2017. Identification and characterization of enzymes catalyzing pyrazolopyrimidine formation in the biosynthesis of formycin A. *Org Lett* 19:1426–1429. <https://doi.org/10.1021/acs.orglett.7b00355>.
25. Burk DL, Hwang J, Kwok E, Marrone L, Goodfellow V, Dmitrienko GI, Berghuis AM. 2007. Structural studies of the final enzyme in the alpha-amino acid pathway-saccharopine dehydrogenase from *Saccharomyces cerevisiae*. *J Mol Biol* 373:745–754. <https://doi.org/10.1016/j.jmb.2007.08.044>.
26. Hong H, Samborsky M, Zhou Y, Leadlay PF. 2019. C-nucleoside formation in the biosynthesis of the antifungal malayamycin A. *Cell Chem Biol* 26:493–501. <https://doi.org/10.1016/j.chembiol.2018.12.004>.
27. Green MR, Sambrook J. 2012. Molecular cloning: a laboratory manual, 3rd ed. Cold Spring Harbor Laboratory Press, Cold Spring Harbor, NY.
28. Kieser T, Bibb MJ, Chater KF, Butter MJ, Hopwood DA. 2000. Practical *Streptomyces* genetics, 2nd ed. John Innes Foundation, Norwich, United Kingdom.
29. Gontang EA, Gaudencio SP, Fenical W, Jensen PR. 2010. Sequence-based analysis of secondary-metabolite biosynthesis in marine actinobacteria. *Appl Environ Microbiol* 76:2487–2499. <https://doi.org/10.1128/AEM.02852-09>.